

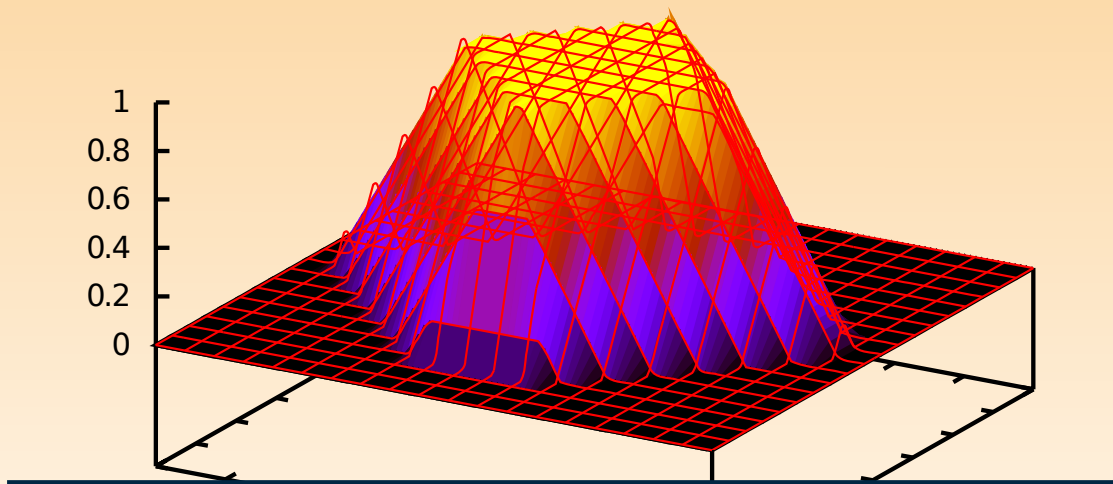
# MTTM

## *Megha-Tropiques Technical Memorandum*

---

**Co-location algorithms**  
Geophysical data projection using  
pixel point spread function

Nicolas Gif, Olivier Chomette, Patrick Raberanto



# Co-location algorithms Geophysical data projection using pixel point spread function

Nicolas Gif, Olivier Chomette, Patrick Raberanto  
Laboratoire de Météorologie Dynamique

September 15, 2011



# Contents

<b>1</b>	<b>Introduction</b>	<b>1</b>
<b>2</b>	<b>Definitions</b>	<b>1</b>
2.1	Point Spread Function . . . . .	1
2.2	PSF weighted co-location . . . . .	2
2.3	Presentation of the spatial co-location methods . . . . .	2
2.3.1	Nagle-like method . . . . .	2
2.3.2	2DI method . . . . .	3
2.4	Pixel descriptions . . . . .	3
2.4.1	MADRAS . . . . .	3
2.4.2	ScaRaB . . . . .	3
2.4.3	SAPHIR . . . . .	4
2.4.4	SEVIRI and GERB . . . . .	4
2.5	Notation . . . . .	5
<b>3</b>	<b>Temporal co-location</b>	<b>5</b>
<b>4</b>	<b>Angular co-location</b>	<b>5</b>
<b>5</b>	<b>Pixel distortion</b>	<b>7</b>
<b>6</b>	<b>Statistics</b>	<b>8</b>
<b>7</b>	<b>Examples</b>	<b>9</b>
7.1	GEO to LEO . . . . .	9
7.1.1	SEVIRI sub-pixel clear area percent coverage to ScaRaB . . . . .	9
7.1.2	GERB to ScaRaB . . . . .	9
7.2	Gridded product to LEO . . . . .	10
7.2.1	IGBP to ScaRaB . . . . .	10
7.2.2	Albedo to ScaRaB . . . . .	11
7.3	LEO to LEO . . . . .	12
7.3.1	CERES to ScaRaB . . . . .	12
<b>8</b>	<b>Documentation</b>	<b>12</b>
<b>9</b>	<b>Conclusion</b>	<b>12</b>
<b>10</b>	<b>Acknowledgments</b>	<b>13</b>
<b>A</b>	<b>Appendix 1 : Integration rules</b>	<b>14</b>
A.1	Monte-Carlo rule . . . . .	14
A.2	Trapezoidal rule . . . . .	14
A.3	Simpson's rule . . . . .	15
<b>B</b>	<b>Appendix 2 : Sensibility tests</b>	<b>16</b>
B.1	Projection of a CERES orbit in a regular grid . . . . .	16
B.2	Projection of a SEVIRI image in an orbit . . . . .	18
B.3	Projection of a GERB image in an orbit . . . . .	19

B.4 Conclusion . . . . .	21
<b>References</b>	<b>22</b>

# 1 Introduction

As part of the mission Megha-Tropiques (MT ; Desbois et al. [2]) and especially for the Scanner for Radiation Budget (ScaRaB ; Kandel et al. [7]), we need to co-locate several times its pixels with pixels of other instruments or gridded geophysical data such as International Geosphere-Biosphere Programme (IGBP) surface type map.

The simplest co-location method, the “nearest-neighbour” method, is not accurate enough for our needs. Thus we use methods that take pixels’ point spread function (PSF) into account (i.e. the real shape of pixels). In this document, we present two spatial co-location methods that are more advanced than the nearest-neighbor one : Nagle-like and 2DI (defined in Section 2.3). These two methods are compared in Section B in terms of quality and CPU time. We show several examples of use of the PSF-weighted co-location in Section 7.

## 2 Definitions

### 2.1 Point Spread Function

The following definition is taken from Dewitte et al. [3].

Consider a continuously varying scene viewed by a satellite instrument (radiometer) with spectral characteristic  $\Phi_{\text{channel}}$ . Let  $\delta_a, \delta_c$  be the angles in two perpendicular directions under which the radiometer views the scene. The radiance measured by the satellite is, assuming linearity of the measurement system, a weighted mean of the continuously varying scene radiances  $L(\text{scene})$ .

$$L_{\text{channel}} = \frac{\int PSF(\delta_a, \delta_c) L(\text{scene}) d\delta_a d\delta_c}{\int PSF(\delta_a, \delta_c) d\delta_a d\delta_c} \quad (1)$$

The weighting function PSF in (1) is called the (total) point spread function (PSF) of the radiometer.

For a scanning radiometer in particular, an along scan angle  $\delta_a$  and a cross scan angle  $\delta_c$  can be considered.

For a cross-track scanning radiometer, the cross-scan direction corresponds to the flight direction of the satellite. The (static) PSF of the radiometer in the non-scanning (static) operation mode is called the optical field of view  $OF_{\text{channel}}(\delta_a, \delta_c)$  of the radiometer. The dynamic PSF of the scanning radiometer is different from the static PSF [11].

If the global time impulse response of the detector (global means: sensor + electronics) is  $h(t)$  and if the instrument is scanning with an angular scan speed  $v_{\text{scan}}$ , the equivalent global angular impulse response of the detector is given by

$$h_{\text{angular}}(\delta_a) = h(v_{\text{scan}} t) \quad (2)$$

The total (dynamic)  $PSF_{\text{channel}}(\delta_a, \delta_c)$  of the detector is obtained by convolution of the optical field of view  $OF_{\text{channel}}(\delta_a, \delta_c)$  with the equivalent angular impulse response  $h_{\text{angular}}(\delta_a)$

$$PSF_{\text{channel}}(\delta_a, \delta_c) = OF_{\text{channel}} * h_{\text{angular}}(\delta_a) \quad (3)$$

## 2.2 PSF weighted co-location

We shall use the term “master” to denote the instrument onto whose footprint the observations of a second instrument, the “slave”, are to be projected.

Let’s consider the following example to illustrate the co-location principle. We want to simulate the data seen by a ScaRaB pixel (green pixel in Figure 1 on page 2) from data provided by a geostationary satellite (red pixels in Figure 1 on page 2).

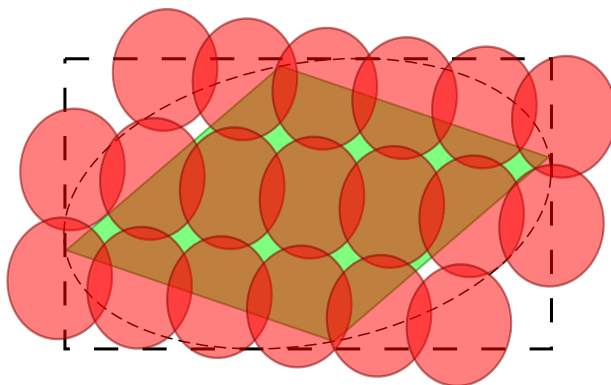


Figure 1: Representation of a square-shaped pixel (green) that overlap with 19 round-shaped pixels. The PSF weighted co-location algorithm calculates the weight of slave (red) pixels inside the master (green) one. No particular scale is respected in this figure.

These pixels have different sizes, shapes, weighting functions, and, as they may be seen from different points of view (two different platforms), their on-ground footprints are distorted in different ways. The PSF-weighted co-location aims to estimate the contribution of each slave (red) pixel inside the master (green) one.

The co-location rely on spherical geometry to take pixels distortion into account. The main part of the geometry formulas are taken from Capderou [1].

To estimate the weights to give to each slave pixel, several integration points are defined in the master pixel domain (dashed rectangle in Figure 1 on page 2) according to the chosen co-location method and integration rules. For each integration point the PSF of the master pixel and the slaves are calculated and accumulated. From these accumulated weights, it is possible to calculate several statistics. The most obvious one would be the arithmetic mean.

## 2.3 Presentation of the spatial co-location methods

### 2.3.1 Nagle-like method

In Nagle and Holz [9], a co-location method is proposed. One considers master pixels as ellipsoids having a linear weighting function going from 1 at the center to 0 at the edge. A weighted mean of the slave pixels whose centers fall in the ellipsoid is made. This method considers the slave pixels as simple points. By adding to this method the possibility to define pixels of any shape and any weighting function (or point spread function), we define the Nagle-like method. We show in Section B that this method is not reliable when slave pixels are not small compared to the master one. In this case one should prefer 2DI method presented below.

### 2.3.2 2DI method

The 2DI method runs through the master pixel's area through an independent integration mesh (not based on slave pixels coordinates). This method gives the possibility to consider slave pixels not just as discrete points, but as also having their own PSF to create a weighting surface whose resolution can be adjusted to the user's needs. This method is interesting when slave pixels have a similar size or are bigger than master pixels. In the other hand, it requires more CPU time. For this method, we implemented three integration rules which are presented in Section A and compared in Section B.

## 2.4 Pixel descriptions

### 2.4.1 MADRAS

Viltard [12] gives the dimensions of MADRAS (Microwave Analysis and Detection of Rain and Atmospheric Structures ; Desbois et al. [2]) instrument's pixels for the different channels. Pixels' cross-scan sizes are 6 km, 10 km and 40 km according to the channel. Figure 3 on page 4 shows a Madras conical swath with pixels of channels 36.5, 23.8 and 18.6 GHz.

### 2.4.2 ScaRaB

ScaRaB instrument's pixel PSF is described in Dewitte et al. [3]. The Figure 2 on page 3 illustrates it.

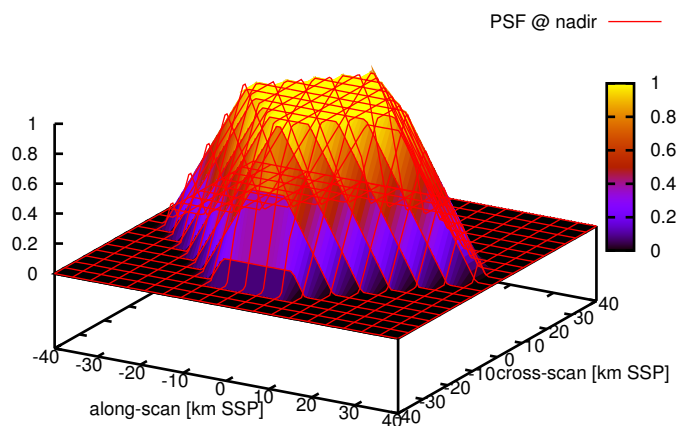


Figure 2: Representation of the ScaRaB instrument PSF. The axis are given in km at sub-satellite point (SSP), assuming the MT altitude is 865.5 km.

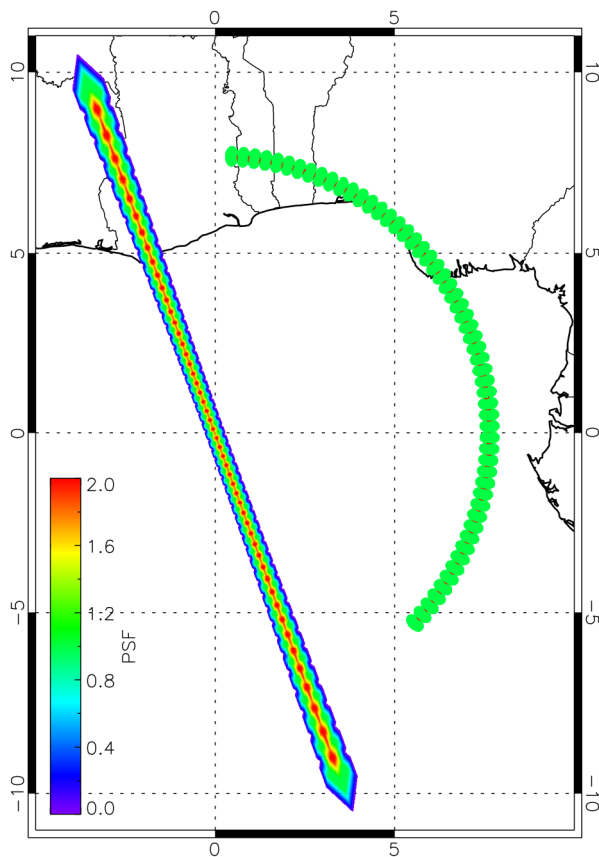


Figure 3: PSF accumulation of the 51 pixels of a ScaRaB MT orthogonal swath and the 56 pixels of a MADRAS MT conical swath. Satellite is situated at  $0^{\circ}\text{N}$ ,  $0^{\circ}\text{E}$ . One can see how the pixels are distorted and overlaps. The MADRAS pixels are modeled by circles of diameter 26.2 km SSP ( $67.25 \text{ km} \times 40 \text{ km}$  once distorted) (Viltard [12]). Pixels positions are provided by Ixion software (Capderou [1]).

### 2.4.3 SAPHIR

The pixels of SAPHIR (Sondeur Atmosphérique du Profil d'Humidité Intertropicale par Radiométrie ; Eymard et al. [4]) instrument are described circles of diameter 10 km SSP. Each othogonal swath is made of 128 pixels.

### 2.4.4 SEVIRI and GERB

SEVIRI (Spinning Enhanced Visible and Infrared Imager ; Schmetz et al. [10]) and GERB (Geostationary Earth Radiation Budget ; Harries et al. [5]) instruments aboard Meteosat Second Generation (MSG) have pinch-shaped pixels (Figure 4 on page 5). SEVIRI pixels are described in Just [6] ; they are 6 km SSP wide. GERB pixels are described in Mueller et al. [8] ; they are 45.5 km SSP wide.



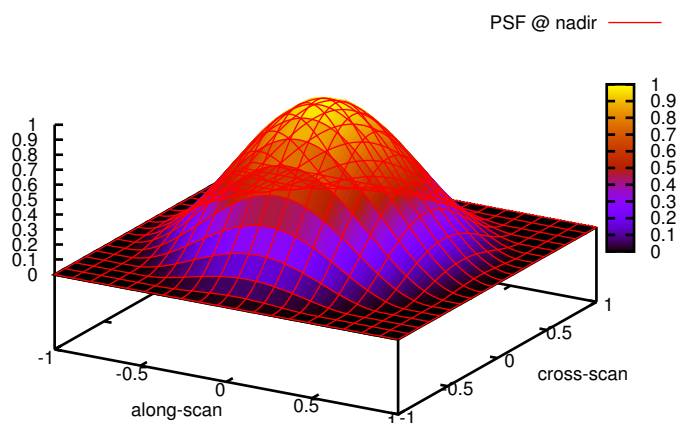


Figure 4: Pinch-shaped PSF of FWHM 1. This one is used for SEVIRI and GERB pixels.

## 2.5 Notation

The following abbreviations would be used in this document :

FWHM : Full Width at Half Maximum

MT : Megha-Tropiques

PSF : Point Spread Function

SSP : Sub-Satellite Point

VAA : Viewing Azimuth Angle

VZA : Viewing Zenith Angle

## 3 Temporal co-location

Slave pixels' selection may also rely on temporal co-location. In this case, one define for each master pixel a time threshold inside the slaves must remains to be co-located.

## 4 Angular co-location

Let's introduce several angles used in this section :

Figure 5 on page 6 shows angles relevant to the satellite's view and swath. The swath angle  $f$  is defined as the angle between the line of sight from the satellite ( $MP$ ) and the nadir ( $MN$ ).

$$f = (MN, MP) \quad (4)$$

The viewing zenith angle  $\zeta$  is the angle at which the satellite  $M$  (or the sun for solar zenith angle) is seen from the surface  $P$ , measured from local vertical.

$$\zeta = (OP, PM) \quad (5)$$

We also use the angle  $\alpha$ , which is the angle at the center of the Earth  $O$  defined by

$$\alpha = (ON, OP) \quad (6)$$

These three angles are related by

$$f + \alpha = \zeta \quad (7)$$

Swath angle and viewing zenith angle are related by

$$\sin \zeta = \eta \sin f \quad (8)$$

where  $\eta$  is the relative altitude of the satellite defined by

$$\eta = \frac{\text{altitude} + R_{Earth}}{R_{Earth}} = \frac{MN + NO}{NO} \quad (9)$$

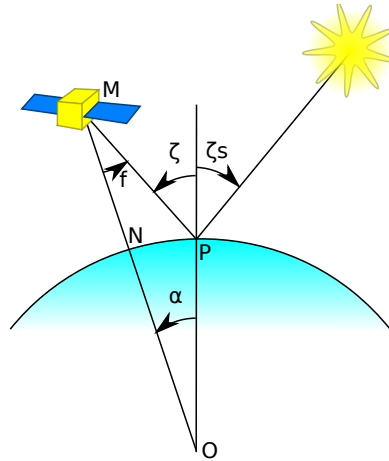


Figure 5: Representation of several viewing and solar angles.  $f$  : swath angle,  $\zeta$  : viewing zenith angle,  $\zeta_s$  : solar zenith angle,  $\alpha$  : angle at the Earth's center.

Figure 6 on page 7 shows azimuth angles. Azimuth angles are defined in the horizontal plane. Viewing azimuth angle  $\beta$  is the angle between north direction and the sub-satellite point  $N$  (or the sun for solar azimuth angle) as seen from  $P$ .

$$\beta = (PNorth, PN) \quad (10)$$

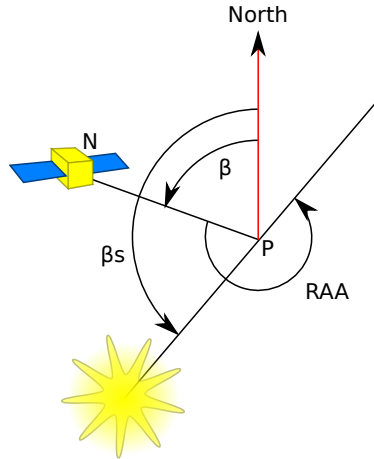


Figure 6: On-ground projection of several viewing and solar angles.  $\beta$  : viewing azimuth angle,  $\beta_s$ : solar azimuth angle, RAA : relative azimuth angle.

In some cases we need to co-locate only pixels observed on particular angular conditions. For example, shortwave radiance emitted by a scene will vary with the viewing zenith angle and viewing azimuth angle. To be compared, the line of sight of two satellites must remain in a cone defined by a maximum scattering angle.

Figure 7 on page 7 shows the scattering angle  $\gamma$ . It is defined from viewing zenith angle  $\zeta$  and viewing azimuth angle  $\beta$  this way :

$$\cos \gamma = \cos \zeta_A \cdot \cos \zeta_B + \sin \zeta_A \cdot \sin \zeta_B \cdot \cos(\beta_A - \beta_B) \quad (11)$$

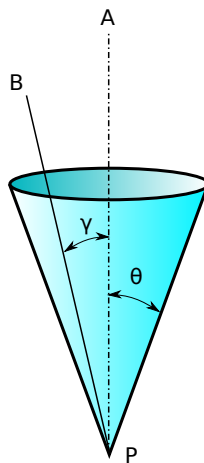


Figure 7: To compare measures observed from a satellite A and a satellite B which observe a point P, the scattering angle  $\gamma$  must be smaller than the threshold  $\theta$ .

## 5 Pixel distortion

The PSF generally depends on the angles in two perpendicular directions under which the radiometer views the scene. One must consider the projection of this function on the ground. The footprint's surface of a pixel will increase as soon as the viewing angle differs from nadir ( $|VZA| > 0$ ).

Here are the expressions that describe pixels' distortion in the direction towards the satellite  $K$  and perpendicularly  $L$  :

$$K(\alpha, \eta) = \frac{1}{\eta - 1} \cdot \frac{\eta^2 - 2\eta \cos \alpha + 1}{\eta \cos \alpha - 1} \quad (12)$$

$$L(\alpha, \eta) = \frac{1}{\eta - 1} \cdot \sqrt{\eta^2 - 2\eta \cos \alpha + 1} \quad (13)$$

where  $\eta$  is the relative altitude (9) of the satellite and  $\alpha$  is the angle at the center of the Earth (6) as shown on Figure 5 on page 6.

## 6 Statistics

At this point we have a list of slave pixels that overlap a master one, the values associated to these and their weights. From this we can calculate a weighted mean :

$$\mu = \frac{\sum_i value_i \cdot weight_i}{\sum_i weight_i} \quad (14)$$

Or the standard deviation :

$$\sigma = \sqrt{\frac{\sum_i ((value_i - \mu)^2 \cdot weight_i)}{\sum_i weight_i}} \quad (15)$$

One can also compute a histogram by accumulating weights of values entering in the same bin. Then the most representative bin is the one having the higher weight. This is particularly useful for discrete data as scene types. As an example, the Figure 8 on page 8 shows a histogram of IGBP 10' resolution product co-located inside a circle of radius 250 km, centered on Mandalay, Myanmar. The mode (12) stands for "Crops".

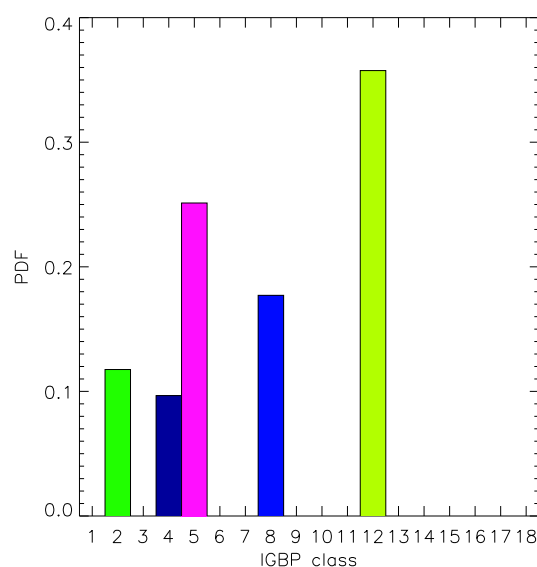


Figure 8: Histogram of IGBP classes, colored by class, co-located 250 km around Mandalay, Myanmar

## 7 Examples

### 7.1 GEO to LEO

#### 7.1.1 SEVIRI sub-pixel clear area percent coverage to ScaRaB

In this example, the PSF-weighted co-location method is used to estimate the ratio of clear-sky SEVIRI pixels inside ScaRaB pixels. Data comes from SAFNWC discrete classifications where clear-sky scenes are given the value “1” and overcast scenes are given value “0”. These zeros and ones are averaged inside each ScaRaB pixel to obtain a continuous value between 0 and 1.

SEVIRI pixels are considered as 6 km SSP FWHM pinches [6].

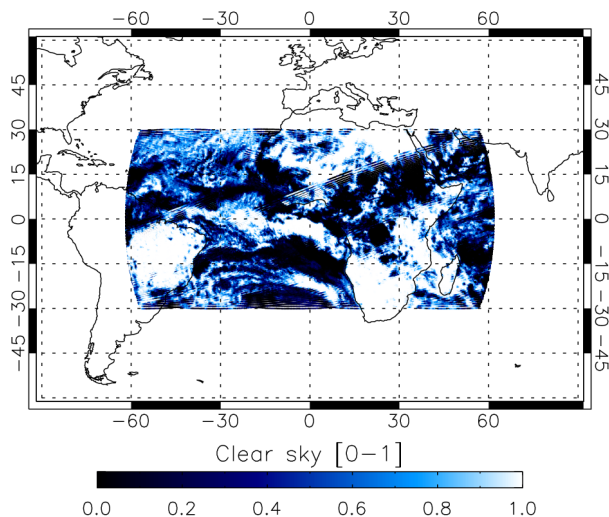


Figure 9: Clearsky ratio in ScaRaB pixels for 1 day (2006-08-13). black = overcast, white = clear

#### 7.1.2 GERB to ScaRaB

GERB pixels are considered as 44.5 km SSP FWHM pinches [8]. The Figure 10 on page 10 is the result of the co-location of a GERB pixel inside a  $1.5^\circ$  box, both centered at 48.436N 2.203E (near Étampes). You can notice how the GERB pixel is distorted.

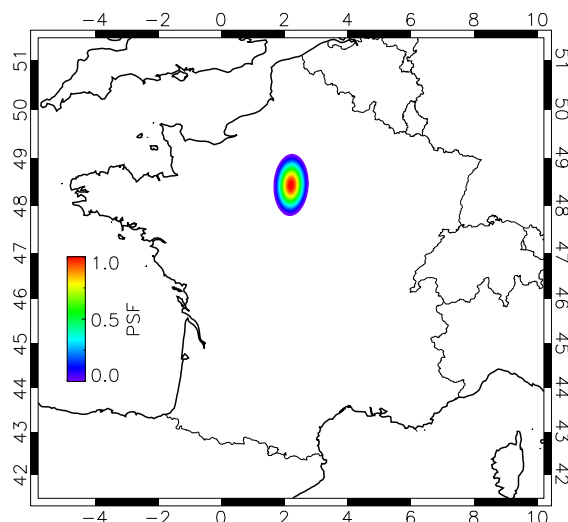


Figure 10: A GERB pixel located at 48.436N 2.203E appears elongated when seen in Mercator projection, colored by PSF

Figure 11 on page 10 shows ScaRaB pixels that match a scattering angle co-angularity (usually used to co-locate short-wave radiances) constrained at  $\pm 5^\circ$  during one MT repeat cycle (7 days)

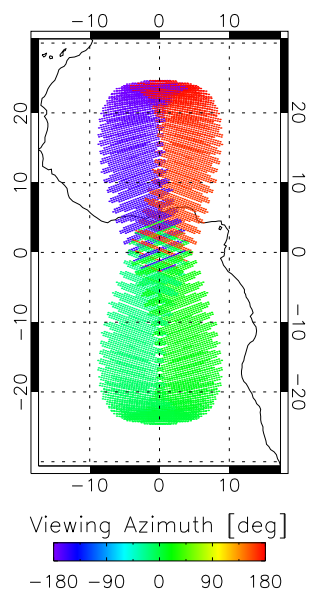


Figure 11: ScaRaB / SEVIRI / GERB matches during 7 days colored by VAA. Scattering angle co-angularity constrained at  $\pm 5^\circ$

## 7.2 Gridded product to LEO

### 7.2.1 IGBP to ScaRaB

The Figure 12 on page 11 is the result of the co-location between a ScaRaB/RESURS orbit and the IGBP 10' resolution scene type product. ScaRaB pixels are given the most representative IGBP value, as explained in Section 6.

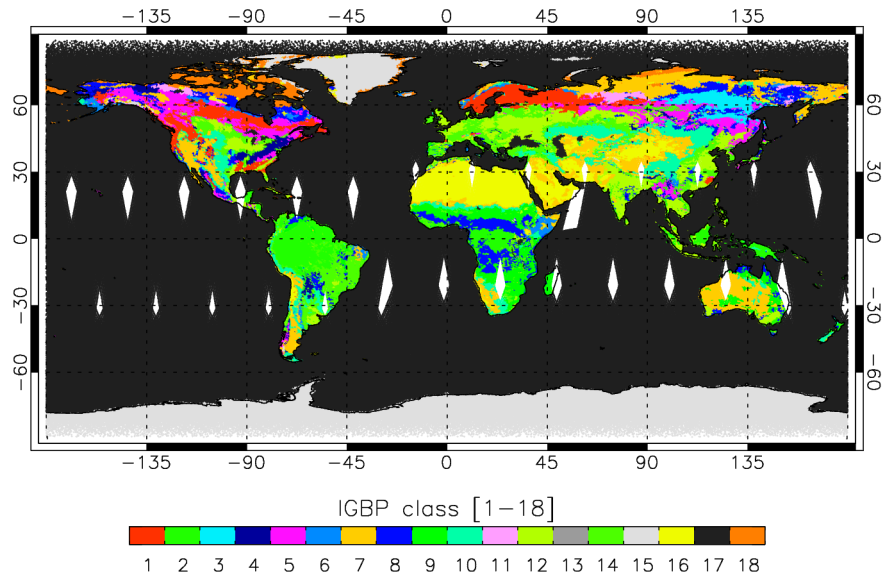


Figure 12: ScaRaB/RESURS co-located during 1 day (1999-03-01) with IGBP 10' resolution product

### 7.2.2 Albedo to ScaRaB

The Figure 13 on page 11 shows the same ScaRaB orbit than in Figure 12 on page 11 co-localized with a 10' resolution albedo product. ScaRaB pixels are given the arithmetic mean of co-located albedo values.

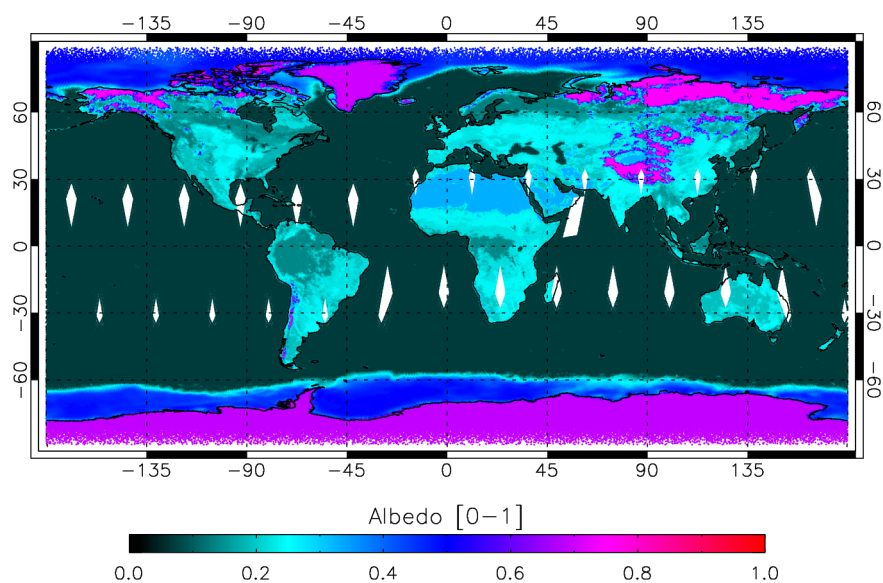


Figure 13: ScaRaB/RESURS co-located during 1 day (1999-03-01) with albedo 10' resolution product

## 7.3 LEO to LEO

### 7.3.1 CERES to ScaRaB

The following example illustrate the VZA angular co-location between ScaRaB (MT) and CERES (Clouds and the Earth's Radiant Energy System ; Wielicki et al. [13]) (Terra) during seven days.

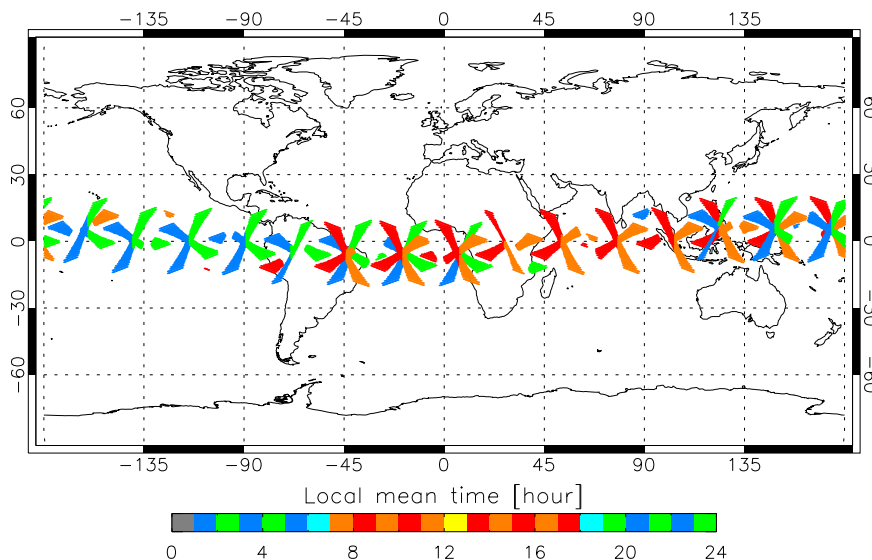


Figure 14: ScaRaB / CERES matches during 7 days  $\pm 5$  minutes, colored by local mean time. Viewing zenith angle co-angularity constrained at  $\pm 10^\circ$  (ie. longwave radiance co-location)

## 8 Documentation

For further technical reference about the usage of the PSF-weighted co-location library's programming interface, consult : <http://www.lmd.polytechnique.fr/~ngif/coloc/html/>

## 9 Conclusion

The presented algorithms are implemented in an object-oriented software library written in C++ (Python interface available thanks to SWIG) which makes it very modular and versatile. Thanks to the abstraction of the code, it is easy to add extra pixel definitions without even seeing or re-compiling the existing part of the code.

It makes possible to co-locate any combination of geophysical data (gridded data, different pixel geometries). According to what is co-located, one method have to be chosen over the other. Nagle-like or 2DI. For this last one, we showed that the trapezoidal integration rule is the best.



## 10 Acknowledgments

For the development of the co-location software library, we thank Michel Capderou for his patience and many precious explanations about angles calculation. We thank Remy Roca for reviewing this document.

## A Appendix 1 : Integration rules

### A.1 Monte-Carlo rule

The Monte-Carlo rule consists in choosing the position of the integration points randomly inside the pixel's domain (dashed rectangle on Figure 1 on page 2).

$$\iint_{\Omega} f(x, y) dx dy = \frac{1}{N} \sum_{i=1}^N f(x_i, y_i) \quad (16)$$

The Figure 15 on page 14 illustrates a way of calculating the surface of a circle with the Monte-Carlo integration.

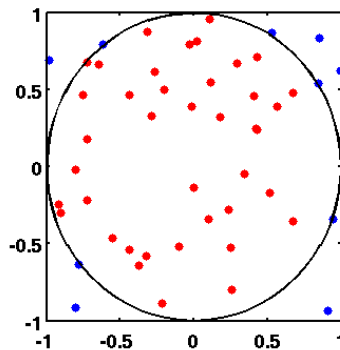


Figure 15: An illustration of Monte Carlo integration. In this example, the domain  $D$  is the inner circle and the domain  $E$  is the square. Because the square's area can be easily calculated, the area of the circle can be estimated by the ratio (0.8) of the points inside the circle (40) to the total number of points (50), yielding an approximation for  $\pi/4 \approx 0.8$  (source: Wikipedia)

For the co-location purpose, we use the pixels' PSF instead of the circle formula of the previous example.

Note that it exists adaptive Monte-Carlo integration methods such as MISER algorithm that will subdivide the domain in equal parts and concentrate the random points in the subdivisions that presents a higher variance.

### A.2 Trapezoidal rule

The trapezoidal rule works by approximating the region under the graph of the function  $f(x)$  as a trapezoid and calculating its area.

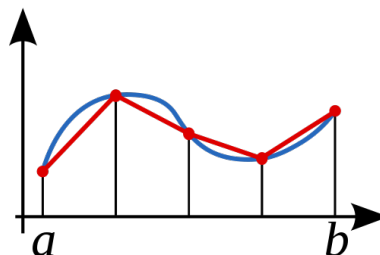


Figure 16: Illustration of the composite trapezoidal rule in 1D (source: Wikipedia)

$$\int_a^b f(x) dx \approx \frac{1}{2} \frac{b-a}{n} \left[ f(a) + f(b) + 2 \sum_{i=1}^{n-1} f(x_i) \right] \quad (17)$$

This method also works for 2-dimensional functions.

The trapezoidal rule consists in meshing the pixel's domain regularly.

$$\int_a^b \int_c^d f(x, y) dx dy \approx \frac{1}{4} \frac{b-a}{m} \frac{d-c}{n} \left[ f(a, c) + f(a, d) + f(b, c) + f(b, d) + 2 \sum_{i=1}^{m-1} f(x_i, c) + 2 \sum_{i=1}^{m-1} f(x_i, d) + 2 \sum_{j=1}^{n-1} f(a, y_j) + 2 \sum_{j=1}^{n-1} f(b, y_j) + 4 \sum_{j=1}^{n-1} \sum_{i=1}^{m-1} f(x_i, y_j) \right] \quad (18)$$

where m and n are the numbers of elements in the mesh in x and y dimension respectively.

### A.3 Simpson's rule

The Simpson's rule works by approximating the region under the graph of the function  $f(x)$  as a quadratic function.

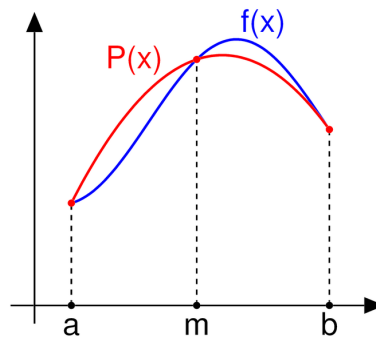


Figure 17: Simpson's rule can be derived by approximating the integrand  $f(x)$  (in blue) by the quadratic interpolant  $P(x)$  (in red) (source: Wikipedia)

## B Appendix 2 : Sensibility tests

The following tests were made with the version 2.15.3 and 2.16 of the co-location library. In this section, the term “Nagle-like” makes reference to the Nagle algorithm improved with custom master pixel PSF and where slave pixels are weighted by their surface.

### B.1 Projection of a CERES orbit in a regular grid

In this test, one projects the CERES (Terra-FM1) orbit of 2006 august the 1st between 13 and 14 UTC in an 1 degree resolution regular grid over Atlantic ocean (60N-60S, 90W-0E at the boxes' edges). The CERES pixels' PSF is based on SSF Collection Guide.

As a reference, the number of integration points per box is raised to 250,000. The arithmetic mean of “Clear Sky Percentage” and “TOA LW Flux” SSF's are calculated.

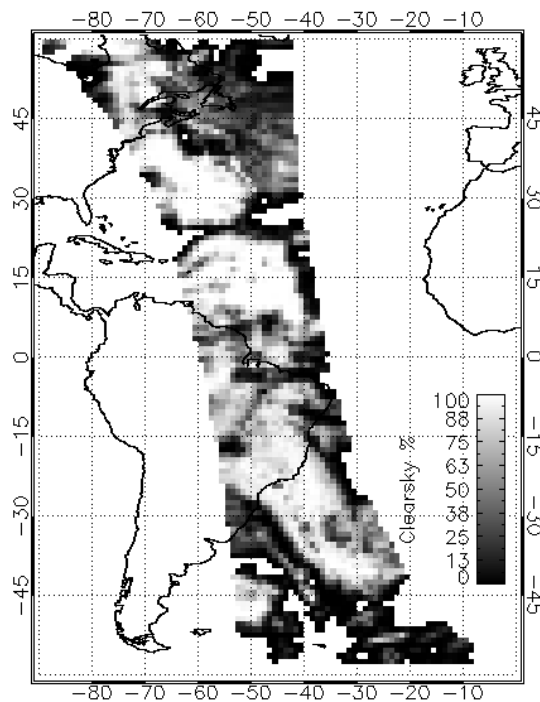


Figure 18: Gridded Clear Sky Percentage

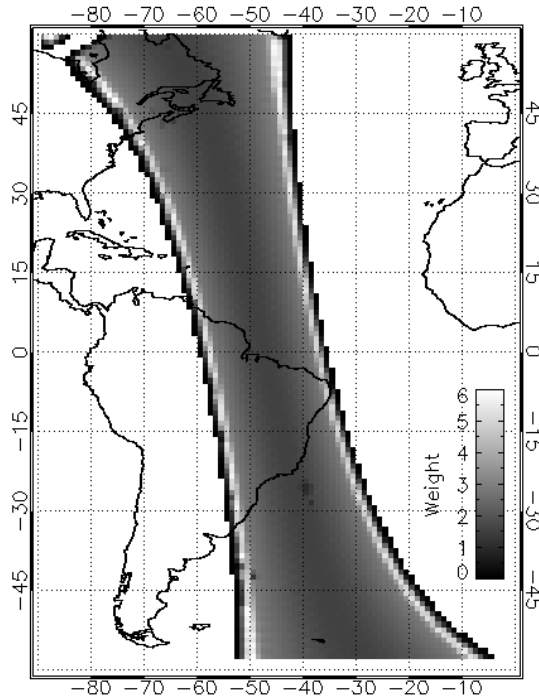


Figure 19: Gridded “Mean PSF”

Mean PSF is calculated this way :

$$\frac{\sum_{i=1}^{nIP} \left( \sum_{j=1}^{nB} (PSF_{B,ij}) \cdot PSF_{A,i} \right)}{\sum_{i=1}^{nIP} (PSF_{A,i})} \quad (19)$$

where index A refers to the master pixel (a 1 degree box here), B refers to the slave pixels (CERES pixels here),  $nIP$  is the number of integration points and  $nB$  the number of slave pixels that overlaps master one. A value of 6 means that 6 “layers” of CERES pixels overlap in the  $1^\circ$  box.

The following statistics give the mean and standard deviation of the difference between the reference (in blue in the tables) and the other runs for the 3582 boxes that have been co-located.

Monte Carlo’s standard deviation is proportional to  $1/\sqrt{N}$ .

Integration pts	2DI				Nagle-like Stdev
	Monte Carlo		Trapezoidal		
	Mean	Stdev	Mean	Stdev	
250000	0,000	0,049	0,000	0,000	2,139
40000	0,000	0,097	0,000	0,029	
10000	0,001	0,188	-0,001	0,052	
2500	0,003	0,368	0,001	0,146	
900	-0,006	0,667	0,001	0,365	
400	0,014	1,014	0,008	0,626	
225	0,024	1,298	-0,002	0,297	
100	0,037	1,989	-0,006	1,307	

Table 1: Clear Area Percentage statistics

Integration pts	2DI				Nagle-like Stdev
	Monte Carlo		Trapezoidal		
	Mean	Stdev	Mean	Stdev	
250000	0,000	0,029	0,000	0,000	1,286
40000	-0,001	0,057	0,000	0,016	
10000	0,000	0,115	0,000	0,028	
2500	0,001	0,241	-0,001	0,075	
900	0,001	0,388	0,000	0,180	
400	0,005	0,567	0,004	0,318	
225	0,002	0,805	0,002	0,166	
100	0,017	1,186	-0,005	0,710	

Table 2: TOA LW Flux statistics

These tables shows that trapezoidal integration rule gives lower biases and standard deviations.

## B.2 Projection of a SEVIRI image in an orbit

Let's see the influence of the number of integration points and the integration rule on the co-location CPU time. In this test, one will project SEVIRI images in a synthetic ScaRaB MT orbit, the 1st of june 2006 between 12 and 13 UTC. Four SEVIRI images are used, co-located at  $\pm 7,5$  minutes.

The given times are CPU times. Real execution time is usually lower since the code take part of multi-core processors.

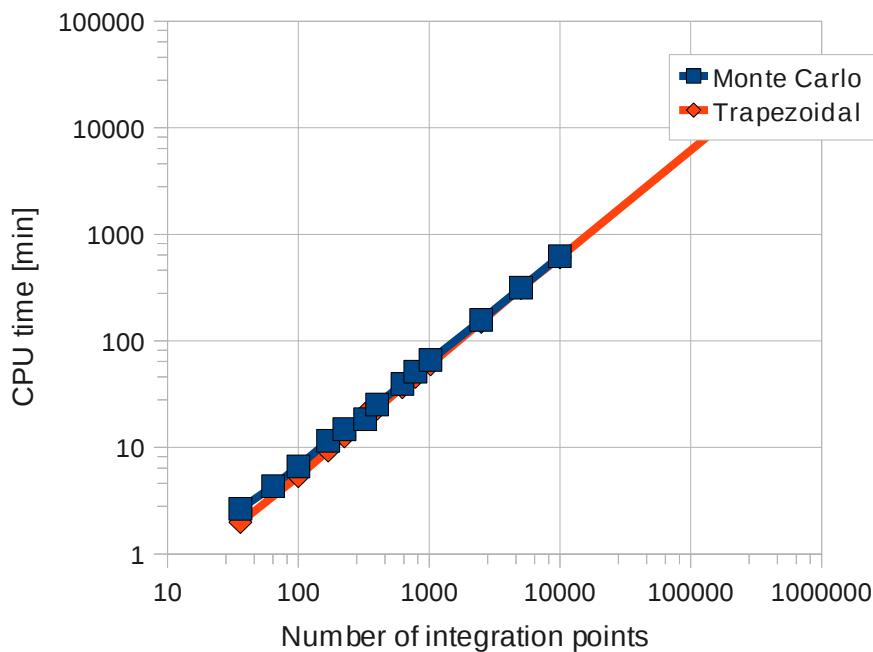


Figure 20: SEVIRI - ScaRaB Co-location CPU times

These results show that in both cases, CPU time is linearly proportional to the number of integration points. Trapezoidal rule is slightly faster than Monte-Carlo.

Integration pts	2DI			Nagle-like
	Monte Carlo	Trapezoidal	Simpson's	
36	3,7	1,48	2,86	0,165
64	2,737	0,694	1,479	
100	2,214	0,374	0,930	
169	1,677	0,164	0,345	
225	1,423	0,109	0,247	
324	1,190	0,053	0,176	
400	1,091	0,037	0,129	
625	0,882	0,023	0,058	
784	0,773	0,015	0,048	
1024	0,686	0,013	0,032	
2500	0,422	0,007	0,010	
5041	0,305	0,006	0,006	
10000	0,205	0,000	0,002	

Table 3: Brightness temperature’s standard deviation VS number of integration points for three 2D integration rules and Nagle-like algorithm

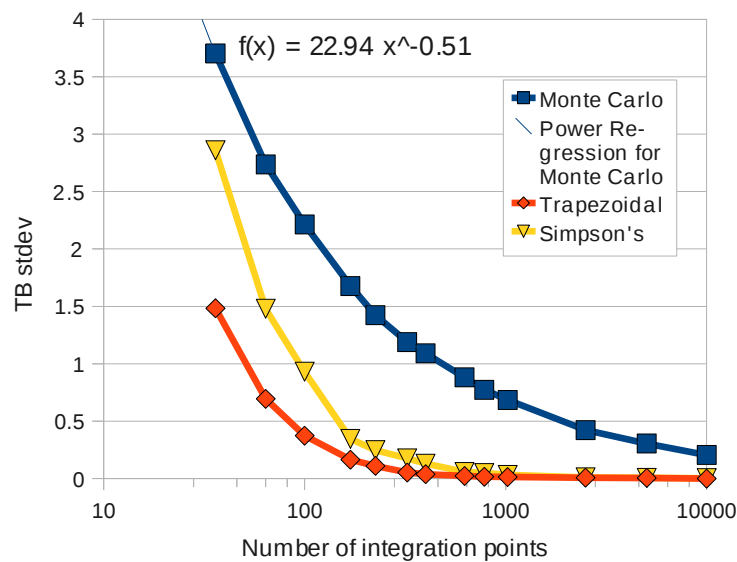


Figure 21: Brightness temperature’s standard deviation

Trapezoidal rule converges faster than other 2D integration rules. Anyway Nagle-like algorithm gives a value as good as 169 integration points with trapezoidal rule for an CPU time more than 16 times shorter.

In this example where SEVIRI’s pixels are small (6 km SSP) compared to ScaRaB’s (40 km SSP), using Nagle-like algorithm is a good choice.

### B.3 Projection of a GERB image in an orbit

Here is the same example than in Section B.2 except we will use GERB images

Let’s notice that GERB’s co-location is about 30 times faster than SEVIRI’s.

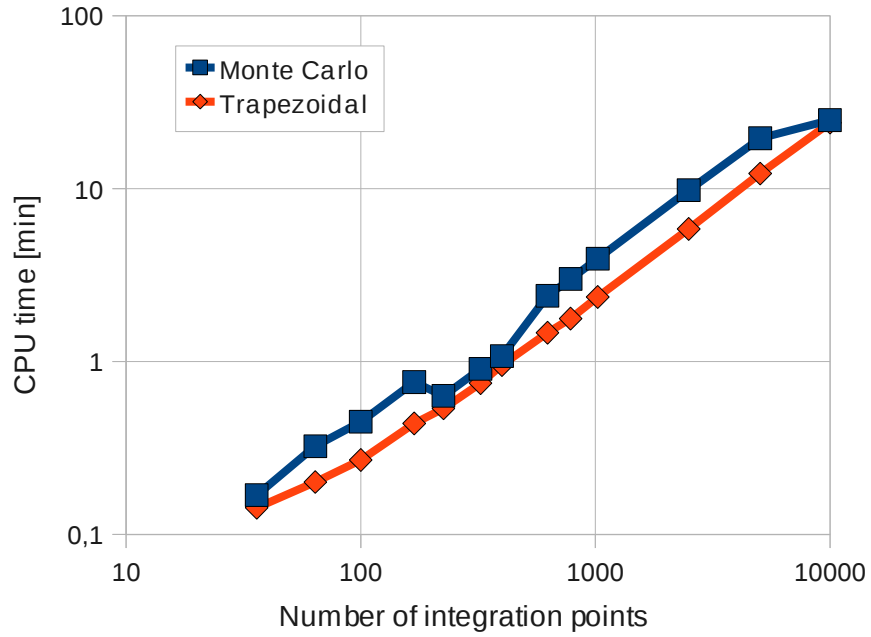


Figure 22: GERB - ScaRaB Co-location CPU times

Integration pts	2DI			Nagle-like
	Monte Carlo	Trapezoidal	Simpson's	
36	2,06	0,31	1,1	4,610
64	1,483	0,067	0,494	
100	1,170	0,031	0,268	
169	0,916	0,014	0,048	
225	0,775	0,007	0,025	
324	0,654	0,006	0,019	
400	0,585	0,004	0,012	
625	0,481	0,002	0,005	
784	0,405	0,002	0,004	
1024	0,377	0,001	0,002	
2500	0,235	0,000	0,001	
5041	0,167	0,000	0,000	
10000	0,120	0,000	0,000	

Table 4: Longwave flux's standard deviation VS number of integration points for three 2D integration rules and Nagle-like algorithm



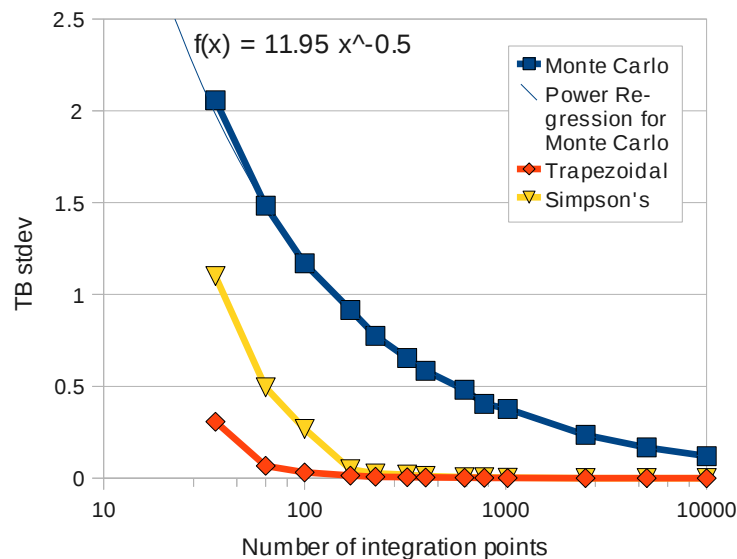


Figure 23: Longwave flux temperature's standard deviation

Here again, Trapezoidal rule is the one which converges the faster. In this example where GERB pixel are as big (45 km SSP) as ScaRaB (40 km SSP) the results given by Nagle-like algorithm are not reliable.

## B.4 Conclusion

This part revealed two points :

1. Nagle-like algorithm can give good results quickly when slave pixels are small compared to master pixels. It is faster since the slave pixels' PSF is calculated only once, at their center, (no need to rotate and distort the pixels). It gives better results because it ensures that all slave pixel are sampled, there is no chance to sub-sample them when there is more of them than integration points. In the other hand, if slave pixels are as big or bigger than master pixel, the 2D integration method should be preferred.
2. If the 2D integration method is chosen, trapezoidal integration rule will give better results than other rules, for the same amount of CPU time.

## References

- [1] M. Capderou. *Satellites, Orbits and Missions*. Springer Verlag, Berlin, Paris, 2005. ISBN 2287213171.
- [2] M. Desbois, M. Capderou, L. Eymard, R. Roca, N. Viltard, M. Viollier, and N. Karouche. *Megha-Tropiques: un satellite hydrométéorologique franco-indien*. 2007.
- [3] S. Dewitte, P. Boekaerts, and F. Sirou. Determination of the ScaRaB FM1 broadband channel point spread functions. *Geoscience and Remote Sensing, IEEE Transactions on*, 37(4):2004–2010, July 1999. ISSN 0196-2892. doi: 10.1109/36.774711.
- [4] L. Eymard, M. Gheudin, P. Laborie, F. Sirou, C. Le Gac, J. P. Vinson, S. Franquet, M. Desbois, F. Karbou, R. Roca, N. Scott, and P. Waldteufel. The SAPHIR humidity sounder. Technical Report 24, IPSL, 2002.
- [5] J. E. Harries, J. E. Russell, J. A. Hanafin, H. Brindley, J. Futyan, J. Rufus, S. Kellock, G. Matthews, R. Wrigley, A. Last, J. Mueller, R. Mossavati, J. Ashmall, E. Sawyer, D. Parker, M. Caldwell, P. M. Allan, A. Smith, M. J. Bates, B. Coan, B. C. Stewart, D. R. Lepine, L. A. Cornwall, D. R. Corney, M. J. Ricketts, D. Drummond, D. Smart, R. Cutler, S. Dewitte, N. Clerbaux, L. Gonzalez, A. Ipe, C. Bertrand, A. Joukoff, D. Crommelynck, N. Nelms, D. T. Llewellyn-Jones, G. Butcher, G. L. Smith, Z. P. Szewczyk, P. E. Mlynczak, A. Slingo, R. P. Allan, and M. A. Ringer. The Geostationary Earth Radiation Budget project. *Bulletin of the American Meteorological Society*, 86(7):945–960, 2011/09/06 2005. ISSN 0003-0007. doi: 10.1175/BAMS-86-7-945. URL <http://dx.doi.org/10.1175/BAMS-86-7-945>.
- [6] D. Just. SEVIRI instrument level 1.5 data. In *First MSG RAO Workshop, 17-19 May 2000*, Bologna, Italy, 2000.
- [7] R. Kandel, M. Viollier, P. Raberanto, J. P. Duvel, L. A. Pakhomov, V. A. Golovko, A. P. Trishchenko, J. Mueller, E. Raschke, R. R. Stuhlmann, and International Scarab Scientific Working Group (Isswg). The ScaRaB earth radiation budget dataset. *Bulletin of the American Meteorological Society*, 79:765–783, may 1998. ISSN 0003-0007. doi: 10.1175/1520-0477(1998)079<0765:TSERBD>2.0.CO;2. URL [http://dx.doi.org/10.1175/1520-0477\(1998\)079<0765:TSERBD>2.0.CO;2](http://dx.doi.org/10.1175/1520-0477(1998)079<0765:TSERBD>2.0.CO;2).
- [8] J. Mueller, R. Stuhlmann, K. Dammann, R. Hollmann, J. E. Harries, S. Kellock, R. Mossavati, R. Wrigley, D. Crommelynck, S. Dewitte, P. Allan, M. Caldwell, and E. Sawyer. GERB: An earth radiation budget instrument on second generation meteosat. *Advances in Space Research*, 24(7):921–924, 1999. ISSN 0273-1177. doi: 10.1016/S0273-1177(99)00356-7. URL <http://www.sciencedirect.com/science/article/pii/S0273117799003567>. Satellite Applications for Energy Budgets and the Hydrological Cycle.
- [9] F. W. Nagle and R. E. Holz. Computationally efficient methods of collocating satellite, aircraft, and ground observations. *Journal of Atmospheric and Oceanic Technology*, 26(8):1585–1595, 2009. doi: 10.1175/2008JTECHA1189.1. URL <http://journals.ametsoc.org/doi/abs/10.1175/2008JTECHA1189.1>.

- [10] J. Schmetz, P. Pili, S. Tjemkes, D. Just, J. Kerkmann, S. Rota, and A. Ratier. An introduction to Meteosat Second Generation (MSG). *Bulletin of the American Meteorological Society*, 83(7):977–992, 2011/09/15 2002. ISSN 0003-0007. doi: 10.1175/1520-0477(2002)083<0977:AITMSG>2.3.CO;2. URL [http://dx.doi.org/10.1175/1520-0477\(2002\)083<0977:AITMSG>2.3.CO;2](http://dx.doi.org/10.1175/1520-0477(2002)083<0977:AITMSG>2.3.CO;2).
- [11] G. L. Smith. Effects of time response on the point spread function of a scanning radiometer. *Applied Optics*, 33(30):7031, October 1994. doi: 10.1364/AO.33.007031. URL <http://ao.osa.org/abstract.cfm?URI=ao-33-30-7031>.
- [12] N. Viltard. Synthesis of the MADRAS characteristics relevant for radiative transfert application. 2007.
- [13] B. A. Wielicki, B. R. Barkstrom, E. F. Harrison, R. B. Lee, G. L. Smith, and J. E. Cooper. Clouds and the Earth’s Radiant Energy System (CERES): An earth observing system experiment. *Bulletin of the American Meteorological Society*, 77(5): 853–868, 1996.

---

# MTTM

Megha-Tropiques Technical Memorandum

---

## **Editorial Committee**

SOPHIE CLOCHÉ

MICHEL CAPDEROU

Laboratoire de Météorologie Dynamique

(LMD / IPSL)

Ecole Polytechnique

F-91128 Palaiseau

France

[Sophie.Bouffies-Cloche@ipsl.jussieu.fr](mailto:Sophie.Bouffies-Cloche@ipsl.jussieu.fr)

<http://meghatropiques.ipsl.polytechnique.fr/available-documents/mttm/index.html>